UNIVERSITY *of York*

This is a repository copy of *Increasing the link-distance of free-space quantum coherent communication with large area detectors*.

White Rose Research Online URL for this paper:
https://eprints.whiterose.ac.uk/173058/

Version: Published Version

Article:

Takedown
If you consider content in White Rose Research Online to be in breach of UK law, please notify us by emailing eprints@whiterose.ac.uk including the URL of the record and the reason for the withdrawal request.

White Rose
university consortium
Universities of Leeds, Sheffield & York

eprints@whiterose.ac.uk
https://eprints.whiterose.ac.uk/

ORIGINAL RESEARCH PAPER

Increasing the Link-distance of Free-space Quantum Coherent Communication with Large Area Detectors

Rupesh Kumar[1,2,3] | Igor Konieczniak[2,3] | Gerald Bonner[4] | Tim Spiller[1,2,3]

[1]Quantum Communications Hub, University of York, Heslington, UK

[2]Department of Physics, University of York, Heslington, UK

[3]York Centre for Quantum Technologies, University of York, Heslington, UK

[4]Fraunhofer Centre for Applied Photonics, Fraunhofer UK Research Ltd, Glasgow, UK

Correspondence

Rupesh Kumar, Quantum Communications Hub, University of York, Heslington, YO10 5DD, UK.
Email: rupesh.kumar@york.ac.uk

Funding information

Engineering and Physical Sciences Research Council, Grant/Award Number: EP/T001011/1; Innovate UK, Grant/Award Number: TS/S009353/1

Abstract

A large area photo-diode based homodyne detector for free-space quantum coherent communication is reported. The detector's performance is studied in terms of the detection bandwidth and electronic noise for shot-noise limited quantum signal detection. Using large area photo-diodes increases the signal collection efficiency from turbulent atmospheric channels, in comparison with the typical fibre-based free-space homodyne detectors. Under identical atmospheric turbulence and receiver aperture conditions, over a 700-km free-space link at 90° elevation angle, our homodyne detector based on a diameter of 1mm photo-diode experiences 0dB loss due to turbulence, while a 10-um fibre-based detector experiences 13.5dB of signal loss.

1 | INTRODUCTION

In coherent communication systems, optical signals carry information on both their amplitude and phase [1]. Coherent detection measures the amplitude and phase of the signal in terms of the quadrature with respect to a strong reference signal called the local oscillator (LO). Since, coherent detectors can differentiate multiple values of signal quadratures, coherent communication has a higher data carrying capacity compare to threshold detection approaches, for example, on-off-keying (OOK), where signal state discrimination is limited to two or a few values. At the lowest intensity levels, near to vacuum, coherent signals evidently show inherent quantum uncertainty in their quadratures. This prevents the different quadrature values being effectively discriminated from each other and hinders data communications. Nevertheless coherent signals at the quantum level are useful for a secure key exchange between two authenticated users [2–4]. However, the coherent detector needs to have a vacuum noise (shot-noise) sensitivity to differentiate signals at the quantum level. Quantum coherent communication for secure key exchange, referred to as the

continuous variable quantum key distribution (CV-QKD) [5], exploits the vacuum noise of the quantum signals to ensure the security of the key. In CV-QKD the quadratures values sent by the transmitter and measured by the receiver are correlated, if properly measured. This correlation can be established through subsequent data reconciliation. Thereafter, error correction followed by privacy amplification are employed to generate a secure key [6].

Degradation in correlation between transmitted and measured quadratures indicates the presence of noise and loss. Vacuum noise of the signal and electronic noise of the detector are two sources of noise that can be calibrated in CV-QKD, whilst the noise from eavesdropping limits the security of the key generation. Attenuation due to the channel and in the receiver, together with detector inefficiency, contribute to the signal loss. In fibre-based systems, the signal is confined in the core of the fibre and signal attenuation is primarily due to absorption/scattering. Many techniques have been proposed and are being developed in order to overcome the losses and to extend the transmission distance, such as measurement device independent (MDI)-QKD [7, 8], use of quantum repeaters [9]

and, most recently, Twin Field (TF)-QKD [10]. All of these methods require an intermediate node(or nodes) between the users.

However, for free-space QKD channels it is quite impractical to extend the overall working link distance by placing a node in between, especially for satellite to ground links [11]. In this article, we are proposing an efficient way to improve the signal collection efficiency in free-space CV-QKD systems, especially for transmitted local oscillator(TLO) based systems. We demonstrate a free-space homodyne detection system with large area photo-diodes and evaluate its effect in CV-QKD operational bandwidth and electronic noise. We show that using larger area detectors, it is possible to achieve higher signal collection efficiency for CV-QKD in atmospheric channels. We have the following sections in this article. In Section 2, we describe the shot-noise sensitive homodyne detection for coherent signals. Section 3 describes the relationship of detector area with bandwidth and electronic noise. In Section 4 we examine the advantage of a large area detector in signal detection compared to single mode fibre-based detectors and provide evidence in terms of shot-noise variance and linear detection response as a preliminary result for conducting free-space CV-QKD demonstration. We conclude the paper in Section 5.

## 2 | CV-QKD OVER FREE-SPACE ATMOSPHERIC CHANNEL

Free-space CV-QKD has recently gained interest primarily because of its capability to filter out noise photons which are not coherent with the LO. This enables daylight operation of QKD in satellite-ground links [12–14]. A few theoretical studies have been carried out in the direction of increasing the loss budget of CV-QKD systems in atmospheric channels. In [15], a realistic and passive eavesdropping scenario is explored, whilst in [12] a virtual aperture is considered as the transmitter of the quantum signals. In this article, we propose a novel concept in quantum coherent signal detection, in order to improve the signal collection efficiency for CV-QKD in atmospheric channels. We also provide preliminary test results to support this proposal.

In a free-space channel, signal loss is not only caused by atmospheric absorption and scattering but also from the beam divergence and by the atmospheric turbulence. The beam divergence is the geometrical spreading of the signal due to diffraction. For short range free-space communications, say a few tens of km, it is possible to keep the beam width of the signal smaller than the receiver aperture. As a result, loss due to the beam divergence is negligible. However, at longer transmission distances, as in the case of satellite to ground links, since the beam width becomes much larger than any practical receiver aperture, only a portion of the signal can in fact be collected.

The portion of the signal collected by the receiver telescope is further coupled to the detector, either via free-space or with fibre pigtails. It is a demanding task as it requires precise pointing, acquisition and tracking (PAT) subsystems and signal focusing optics in order to keep the signal focused onto the detector area, which has typical diameters of 10 μm in the single mode fibre, 80 μm in the multi-mode fibre and 200 μm in the free-space detector. Random variations of the refractive index of the atmosphere generate scintillation effects that results in signal fading, wavefront distortion and random motion of the signal beam centroid about the receiver. After all, the atmospheric turbulence spreads the signal spot size and reduces the signal collection efficiency significantly. Adaptive optical techniques can correct the wavefront distortion and increase the signal coupling efficiency to the detector with an aid from beacon signal, at a separate wavelength, that is transmitted along with the QKD signal [12]. Precision telescopic mounts with high tracking resolution can follow the wandering signal beam. However, this compromises in tracking speed [16].

We have considered only the scope of TLO based CVQKD systems in our analysis. The performance of locally generated LO (LLO) based systems is limited to shorter working transmission distances, due to the phase noise that arises from two independent lasers. Narrow linewidth (<1 kHz) lasers that offer lower phase noise are costly, bulky and require precise temperature and current control. These are thus unlikely to provide an optimal solution for transmitters with size, weight and power (SWaP) restrictions. As in the case of classical coherent communications, a higher detection bandwidth is required for conventional wide linewidth lasers (>1 MHz), to estimate the phase of the reference pulse precisely. As can be seen in Figure 3, the electronic noise increases with the detection bandwidth. This makes the detection thermal noise limited rather than shot noise limited. It is not possible to compensate for this by increasing a locally sourced LLO power, because adjusting the receiver to be shot noise limited would require LLO power that will saturate and
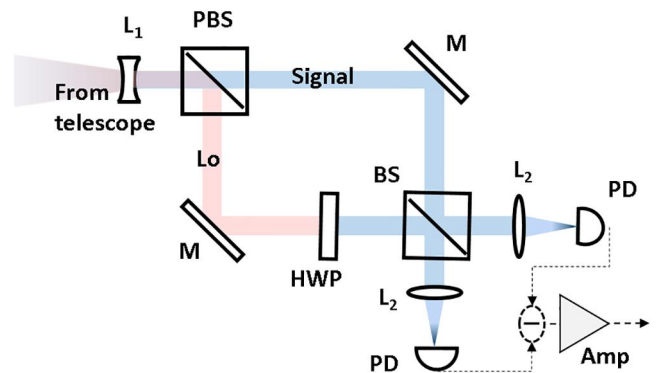

FIGURE 1 Set-up for the free-space homodyne detection. Focused signal from the primary mirror of the telescope is first collimated by lens L1 and then passes through the polarization beam-splitter (PBS) for separating the orthogonal polarized signal and LO. Polarization of the LO is rotated with half wave plate (HWP) to match with that of signal. The signal and LO interfere at a 50/50 beam-splitter (BS) and its outputs are each focused to a photo-diode (PD) using lens L1 and L2. M stands for the mirror

damage the photodiodes. Therefore, larger area based detectors find their application in TLO (rather than LLO)-based CVQKD systems. The use of larger area photodiodes not only reduces the need for precise beam stabilization and reduces design complexities as well as cost, but it also improves the signal collection efficiency.

3 | QUANTUM COHERENT SIGNAL DETECTION

Since the signal strength is comparatively higher, a classical coherent detector has diverse detection capabilities—in terms of orthogonal polarizations for both quadratures. On the contrary, quantum coherent signals are very weak in intensity - a few photons per pulse on average at the transmitter [6]. Diversified signal detection over a lossy channel creates further loss. Therefore, quantum coherent signals are prepared in a single polarization and detected preferably in a single quadrature. Single quadrature detection is referred to as homodyne detection, whilst detection of both quadratures is termed heterodyne. Based on the protocol for secure key generation, the CV-QKD detector either randomly measures one of the quadratures, or measures both quadratures. We consider a homodyne detector in our analysis primarily because of its use in a well-studied and demonstrated Gaussian modulated coherent state (GMCS) protocol [5, 6] for CV-QKD.

In the homodyne detection for quantum signals, the signal field $\alpha e^{i\theta_s}$ is mixed with a strong LO field $\sqrt{I_{lo}}e^{i\theta_{lo}}$ on a symmetric beam-splitter as shown in Figure 1. Here α is the complex amplitude and I_{lo} is the intensity of the LO. The signal can be expressed in terms of field quadratures, $X + iP$. Since the LO and signal originate from the same laser source in TLO-based CV-QKD systems, the signal quadrature with respect to the LO can be written as $(X_{\theta_{lo}} + X_0) + i(P_{\theta_{lo}} + P_0)$. Here, X_0 and P_0 are the random quadrature values correspond to vacuum noise variance which does not have any phase relation with the LO. The outputs of the beam-splitter are connected to photo-diodes. The photo-currents are subtracted from each other and the difference is amplified to a detectable level. The amplifier output directly indicates the quadrature of the input signal where the relative phase of the LO with respect to the signal determines the quadrature under measurement.
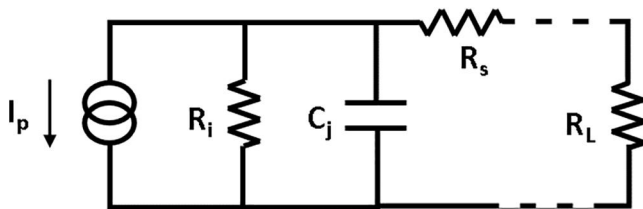
FIGURE 2 Equivalent circuit of a photo-diode. C_j is the junction capacitance, R_i is the internal resistance and R_s is the series resistance, R_L is the load resistance and I_p is the photocurrent

The homodyne detection output, HD_{out}, for an X quadrature measurement (and similarly for the P quadrature) can be written as:

$$HD_{out} = 2\sqrt{I_{lo}}(X_{\theta_{lo}} + X_0) + X_{ele} \tag{1}$$

where, X_{ele} is the noise quadrature contribution due to the electronic noise variance V_{ele}. The signal quadrature $X_{\theta_{lo}}$ may contain excess noise that originates from other sources, which we are neglecting in our analysis. The shot-noise limited sensitivity of the homodyne detector is obtained using a high intensity LO and low electronic noise generating components—photodiodes and amplifier. Primarily, the electronic noise variance determines the intensity required for the LO to bring the homodyne detector to shot-noise sensitivity. Therefore, it is important to evaluate how the electronic noise varies with different aspects of the detector.

4 | HOMODYNE DETECTOR WITH LARGE AREA PHOTO-DIODES

In general, there are three figures of merit for a receiver: detection efficiency, bandwidth and electronic noise. Detection efficiency is the product of the quantum efficiency of the photo-diodes and the optical loss in the receiver including the telescope. The detection bandwidth of the receiver is bounded by the electrical bandwidth of the photo-diode and the amplifier. This is relevant as it can limit the signal repetition rate. Typically repetition rate is set to one-third of the bandwidth and signal pulse width is to 10% of the duty-cycle [17]. In order to make the homodyne detector shot-noise sensitive, it is required to have comparatively low electronic noise from the detection electronics—the third term in Eq.(1). Its contribution can be made smaller either by higher LO intensity, I_{lo}—the first term in Eq.(1), or using low noise electronic components at the expense of the reduction in the bandwidth. In a homodyne detector, the bandwidth, B, and electronic noise variance, V_{ele}, are related by the following equation [18].

$$V_{ele} = \frac{NEP^2 B\tau}{h\nu I_{lo}} \tag{2}$$

where, NEP is the sum of the noise-equivalent power of the photo-diodes and the amplifier, τ is the LO pulse width, h is Planck's constant and ν is the optical LO frequency.

In our noise model, we consider the NEP of the amplifier to be constant and analyse how the detection area of the photo-diode affects the NEP, bandwidth and thence the electronic noise variance. In order to relate the area of the photo-diode to bandwidth, we consider the equivalent circuit of a photo-diode as shown in Figure 2. For a photo-diode with junction capacitance C_j connected to a load resistor, R_L, the bandwidth $B = 1/2\pi R_L C_j$ can be expanded as:

$$B = \frac{1}{\pi R_L A} \sqrt{\frac{\mu \rho (V_A + V_{bi})}{2 \epsilon \epsilon_0}} \qquad (3)$$
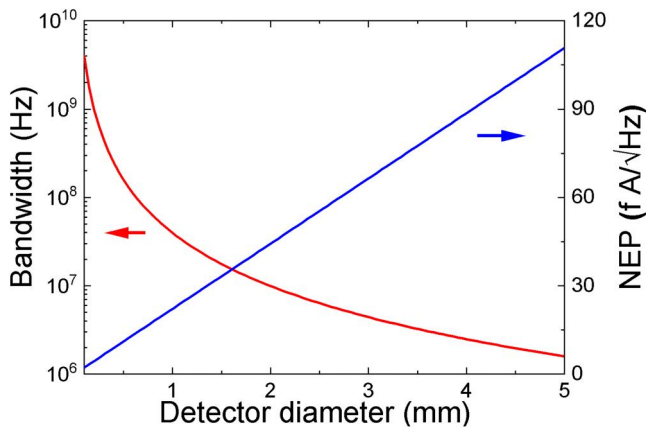
where A is the detection area of the diode, μ is the mobility of electrons at 300K, ρ is the resistivity of the photo-diode material, V_A is the built in potential of the material, V_{bi} is the applied reverse bias voltage, ϵ is the dielectric constant and ϵ_0 is the permittivity of free space. As the area of the detector increases the detection bandwidth reduces, due to increase in junction capacitance, as shown in Figure 3.

Considering the dark current as the source of noise in the photo-diode, the NEP can be defined as the power required to generate a photo current equivalent to that of the dark current, which can be written as [19]:

$$NEP = \frac{I_0 \left[e^{q V_A / kT} - 1 \right]}{\gamma * \sqrt{B}} \qquad (4)$$

where the term in the numerator is the dark current, γ is the quantum efficiency of the PIN diode, and $I_0 = \frac{q A n_i^2}{N_A} \left[\frac{kT \mu_n}{q \tau_n} \right]^{1/2} \tanh\left(\frac{t}{L_n}\right)$ is the saturation current, applied in the equation as its root mean square value. Here N_A is the electrically active acceptor/hole concentration on the lightly doped p-side of the junction, n_i is the intrinsic carrier concentration, A is the junction area, τ_n is the minority carrier lifetime, μ_n is the minority carrier mobility, L_n is the minority carrier diffusion length, t is the thickness of the p-type base of the diode, and V_{bi} is the bias voltage across the diode. T, q and k are, respectively, the temperature, the charge of the electron and the Boltzmann's constant.

In Figure 3 the red line shows the variation of the bandwidth of the photo-diode with respect to the diameter. The bandwidth primarily reduces due to the increase in junction capacitance of the photo-diode with detection area. The blue line shows the variation of NEP of the photo-diode. It is evident from the graph that the noise from the photo-diode increases with respect to the diameter. By inserting Eq.(3) and Eq.(4) in Eq.(2), we can summarise that electronic noise variance increases with the detection area of the photo-diodes as shown in Figure 4.

Since, most of the CV-QKD systems are demonstrated at around a few MHz clock rate, we consider 10 MHz bandwidth amplifier with $NEP = 5 \times 10^{-12} W/\sqrt{Hz}$. Even though the electronic noise increases and overall bandwidth decreases, it is still manageable to achieve MHz clock rates with a 3-mm diameter detector, see Figure 3, under the assumption that the clock rate is one-third of the homodyne bandwidth. We have also provided an example of 100 MHz with a $NEP = 10^{-11} W/\sqrt{Hz}$ amplifier. As expected, the electronic noise variance is higher compare to 10 MHz, due to higher amplifier NEP. Note that the maximum clock rate, 33 MHz at one-third of the total bandwidth, cannot be achieved with a detector diameter larger than 1 mm.

5 | PERFORMANCE OF LARGE AREA PHOTODIODE HOMODYNE DETECTOR

We have seen in the previous section that increasing the detection area of the photo-diode decreases the detection bandwidth and increases the electronic noise variance. In this section we will analyse the advantages of using a large area detector in a free-space CV-QKD link. Transmission of signal through a free-space channel creates signal loss due to beam divergences. One way to decrease the signal divergence is to use a large aperture telescope at the transmitter as per the following relation with the divergence angle $\Theta = 1.22 \lambda / D$,
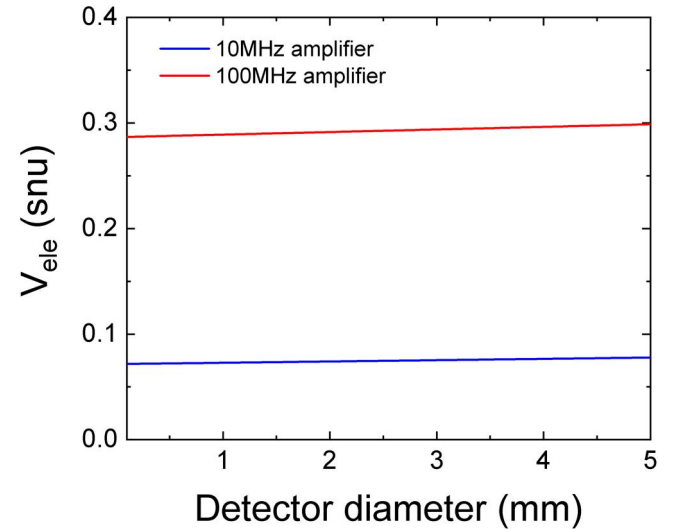

FIGURE 3 Variation of the bandwidth (red line) and NEP (blue line) with respect to the diameter of the photo-diode. The following values are used in Eq.(3) and Eq.(4): $R_L = 50\ \Omega$; $\mu = 10^4 \frac{cm^2}{Vs}$; $\rho = 0.142\ cm\Omega$; $V_A = 0.77\ V$; $V_{bi} = 6V$; $\epsilon = 13.9$; $n_i = 6.3 \times 10^{11}\ cm^{-3}$; $N_A = 1.2 \times 10^{31}\ cm^{-3}$; $T = 300K$; $\mu_n = 250\ cm^2/(vs.)$; $\tau_n = 270 \times 10^{-15}s$; $t = 55\ cm$; $L_n = 14\ nm$; $\gamma = 95\%$

FIGURE 4 Variation of the electronic noise variance with respect to the detector diameter. The blue and red lines represent the cases of 10 MHz and 100 MHz bandwidth for the amplifiers. The following values are used in Eq. (2): $NEP_{amp} = 5 \times 10^{-12}\ W/\sqrt{Hz}$ and $10^{-11}\ W/\sqrt{Hz}$; $\tau = 0.3 * B^{-1}$; $I_{lo} = 13\ \mu W$

where λ is the wavelength of the signal and D is the diameter of the transmitter telescope [20]. For transmission over short distances, the beam diameter can be maintained below a typical receiver telescope diameter (say, 40 cm diameter) by using a suitably large transmitter aperture. For example, over a 10-km free-space link, an 8-cm transmitter aperture produces a 24-cm beam diameter at the receiver, resulting in negligible diffraction losses. In the case of a satellite-to-ground link, as the transmitter aperture is limited by the size of the satellite, and in any case, impractically large transmitter and receiver apertures would be required due to the very large distance (hundreds of kilometres even for low Earth orbits).

In either case, in addition to any losses due to diffraction, atmospheric turbulence can cause further losses due to spreading and wander of the beam caused by spatially and temporally random variations in the refractive index of the air. In order to compare the large area detector with fibre-coupled detectors, we have modelled the propagation of the signal beam through the atmosphere for the case of a satellite-to-ground link, and calculated the coupling losses for both types of detector. Atmosphere turbulence is described statistically. The stochastic behaviour of the refractive index is determined by the structure function $D_n(r) = C_n^2 r^{2/3}$, which describes the expectation value of the difference in refractive index between two points a distance r apart, where the term C_n^2 referred as refractive index structure parameter [21]. C_n^2 is thus a measure of the strength of the turbulence, and is typically in the range 10^{-16} to $10^{-12} \mathrm{m}^{-2/3}$ at ground level. The strength of the turbulence decreases significantly with altitude, and in the present calculations we have used the Hufnagel-Vally model for the variation of C_n^2 with altitude [21].

The case of a satellite in a 700-km low Earth orbit at an elevation of 90° was considered. The 1550 nm signal beam was launched with a $1/e^2$ diameter of 7.1 cm, and a divergence of 14 microradians. The ground level turbulence of $10^{-13 \mathrm{\,m}-2/3}$ and a high altitude wind speed of 21 m s^{-1} were assumed as inputs to the Hufnagel-Valley turbulence profile. The atmosphere was divided into 14 slices, each of which was modelled by propagation over the thickness of the slice and a random phase screen calculated based on Von Karmen statistics using the AOtools Python package [22]. Specifically, the function aotool.turbulence. phasescreen.ft_phase_screen was used to generate the phase screens, with the outer and inner scales, L_0 and l_0, set to 100 and 0.01 m respectively, and r_0 calculated from the thickness of the slice and the value of C_n^2 at that altitude, as determined from the Hufnagel-Valley turbulence profile. To determine the long-term average losses, the model was run 800 times, with the phase screens seeded with random numbers on each iteration to build up the statistical variation of the turbulence under the conditions described above. Fourier optics techniques were used to propagate the electric field to the plane of the detector/fibre facet, through the receiver, which had an aperture of 35.5 cm and an effective focal length of 1600 mm. A 10-μm diameter single-mode fibre and a square detector of side 1 mm were considered. Note that the parameters considered here are typical examples for a modest satellite in low Earth orbit since our aim is to provide evidence to the improvements in signal collection

efficiency while using large area photo-diodes. However, the effective focal length was chosen to optimise coupling into the fibre (about 80% coupling efficiency) in the case of no turbulence. For a fair comparison between fibre based and free-space photodiode detection, we have considered identical telescope parameters. The choices of the aperture and focal length of the telescope are arbitrary, however, these are taken to be consistent with a standard telescope.

The inset of Figure 5 shows the focal plane of the receiver telescope with fibre and large area detectors under a weak turbulence conditions. It is visually evident that the large area detector can collect more light and thereby reduces the signal loss. One important thing to note here is that, since the LO and signal undergo identical turbulence effects, the spatial profile of the signal is identical with that of the LO. As a result, the signal is mode matched and coherent with respect to the LO—a requirement for efficient homodyne detection.

The average losses due to turbulence alone were 13.5 dB in the case of the fibre, while the large area detector easily collected all the light passing through the receiver aperture, with 0 dB of turbulence-induced losses; in that case only the diffraction losses of 31.8 dB suffered. (atmospheric absorption and scattering was not considered here.) We have also considered the field-of-view of the receiver in terms of detector area and telescopes focal length, f, given by $2\tan^{-1}(\sqrt{A/\pi}/f)$. The fibre facet has a field-of-view in this case of 6.25 microradians, while the 1-mm detector has a field-of-view of 625 microradians for the present focal length. In practice, one could significantly increase the focal length of the receiver and still collect all or most of the signal light passing through the aperture, whilst reducing the field-of-view to minimise background noise. This gives substantially a more design freedom. And also, larger field-of-view reduces the resolution requirement for the mount for
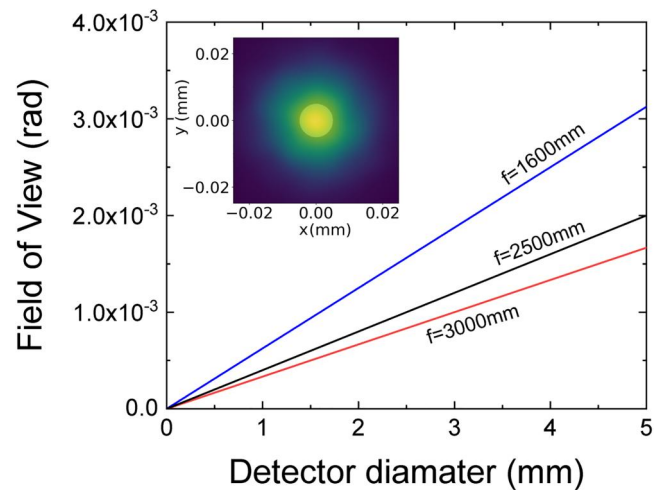
FIGURE 5 Field-of-view versus detector diameter. Field-of-view is estimated for different focal length of the telescope. The figure in the inset shows received signal intensity profile under moderate turbulence on a 10-um core diameter of the single mode fibre (indicated by the paler circle at the centre of the figure inset). A large area detector easily collects all the light - the square region shows only the central 50 μm of the 1 mm detector
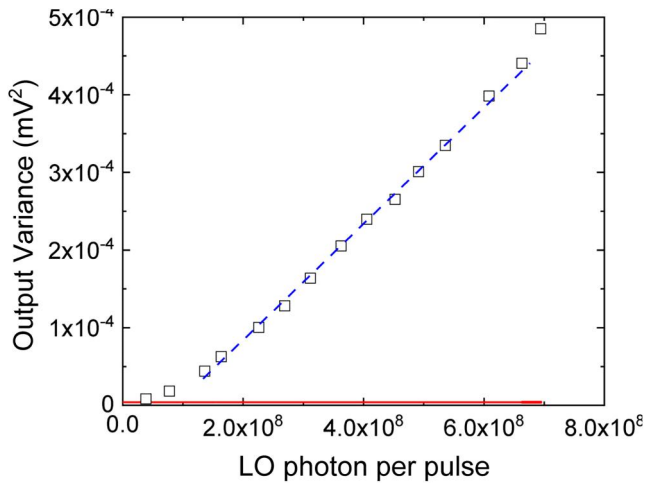
FIGURE 6 Output variance of the homodyne detector at various local oscillator powers. The blue dashed lines are added to indicate the linear region for the detector. The red solid line is the electronic noise variance measured without the LO

tracking the transmitter. As long as the lateral beam displacement is within the area of the photo-diodes, precise beam stabilization is also not required, as the signal and LO are subjected to the same displacement.

In order to evaluate the shot-noise sensitivity of the large area detector based homodyne detector, we have performed the following test. A 30-ns wide laser pulse of wavelength 1550 nm at 1 MHz rate is used as the LO pulse for the homodyne detector with 1 mm diameter photo-diodes. The photo-currents from both photo-diodes are made equal by balancing the homodyne detector. The output variance is measured, without signal, at various LO intensities. Electronic noise variance of the detector is also measured without the LO. The measurement result is shown in Figure 6. The homodyne detector shows linear response with respect to the LO power. For the case of TLO systems, the link loss in the channel will reduce the LO intensity at the receiver, which could lead to the homodyne detector being thermal noise limited rather than shot noise limited. However, utilising intense laser sources at the transmitter, which are required for other practical aspects of the communications such as PAT, can mitigate this problem. For example, over a 31.8dB loss channel, a 100 ns laser pulse of 1W peak power at the transmitter contains 5.5×10^8 photons per LO pulse at the receiver. Similarly, over a 40-dB loss channel, a 5-W laser will produce 4.2×10^8 photons per 100 ns LO pulse at the receiver. One can also modify the pulse width to increase the number of photons per LO pulse at the receiver, to make sure that the detector is shot noise limited.

6 | CONCLUSION

We have shown that using large area photo-diodes increases the signal collection efficiency under atmospheric turbulence compared to a fibre-based signal receiver. Considering loss from beam divergences and atmospheric turbulence, a fibre-based receiver experiences 45.3dB loss while a 1 mm detection shows 31.8dB loss from a 700-km satellite to ground link at 90°. Our homodyne receiver evaluation shows a linear shot-noise limited sensitivity at the reduced bandwidth, however, still adequate for performing CV-QKD at typical MHz clock rates. Such a receiver will also reduce the need for precision telescopic mount controls for a static link where the transmitter and the receiver are stationary or station-keeping. A noticeable feature of the large area detector-based homodyne detector is that the it obviates the need for adaptive optical elements in the free-space link. Larger field-of-view is another benefit of using large area photo-diodes, however, this increases the background noise photon flux. Since the LO works as a mode selector for the quantum signals, higher FOV may not have a significant effect on the CV-QKD systems. However, the effect of comparatively lower LO power may reduce the noise photon rejection ability of the homodyne detector. We will analyse the effect of the large FOV at a secure key rate in our future study.

ORCID
Rupesh Kumar https://orcid.org/0000-0002-6813-6401
Igor Konieczniak https://orcid.org/0000-0003-1519-5819

REFERENCES
1. Kikuchi, K: Fundamentals of coherent optical fiber communications. J. Light. Technol. 34, 157 (2016)
2. Gisin, N., et al.: Quantum cryptography. Rev Mod Phys. 74, 145–195 (Mar 2002)
3. Diamanti, E., Anthony, L.: Distributing secret keys with quantum continuous variables: Principle, security and implementations. Entropy. 17, 6072–6092 (2015)
4. Xu, F., et al.: Secure quantum key distribution with realistic devices. Rev Mod Phys. 92(2), 025002 (2020)
5. Grosshans, F., Grangier, P.: Continuous variable quantum cryptography using coherent states. Phys Rev Lett. 88, 057902 (Jan 2002)
6. Paul, J., Kunz-Jacques, S., Anthony, L.: Long-distance continuous-variable quantum key distribution with a Gaussian modulation. Phys. Rev. A. 84, 062317 (Dec 2011)
7. Samuel, L., Stefano, P.: Side-channel-free quantum key distribution. Phys Rev Lett. 108, 130502 (2012)
8. Lo, H.-K., Curty, M., Qi, B.: Measurement-device-independent quantum key distribution. Phys Rev Lett. 108, 130503 (2012)
9. Duan, L.-M., et al.: Long-distance quantum communication with atomic ensembles and linear optics. Nature. 414, 413–418 (2001)
10. Lucamarini, M., et al.: Overcoming the rate-distance limit of quantum key distribution without quantum repeaters. Nature. 557, 400 (2018)
11. Bedington, R., et al.: Progress in satellite quantum key distribution. npj Quantum Inf. 3, 30 (2017)
12. Kevin, G., et al.: Quantum-limited measurements of optical signals from a geostationary satellite. Optica. 4(6), 611–616 (2017)
13. Guo, Y., et al.: Channel-parameter estimation for satellite-to-submarine continuous-variable quantum key distribution. Phys. Rev. A. 97, 052326 (2018)

14. Hosseinidehaj, N., et al.: Satellite-based continuous-variable quantum communications: state-of-the-art and a predictive outlook. IEEE Communications Surveys Tutorials. 21(1), 881–919 (2019)

15. BahraniGhalaii, S.M., et al.: Psatellite quantum key distribution under restricted eavesdropping scenarios. In: qcrypt19. Montreal (2019)

16. Baister, G., Gatenby, P.V.: Pointing, acquisition and tracking for optical space communications. Electron Commun Eng J. 6(6), 271–280 (1994)

17. Tang, X., et al.: Intersymbol-interference reduction in continuous variable QKD using equalization. In: IEEE Globecom Workshops (GC Wkshps). Abu Dhabi (2018)

18. Tang, X., et al.: Performance of continuous variable quantum key distribution system at different detector bandwidth. Optic Commun. 471(15), 126034 (2020)

19. Gopal, V.: A new approach to investigate leakage current mechanisms in infrared photodiodes from illuminated current-voltage characteristics. J Appl Phys. 116, 084502 (2014)

20. Kerstel, E., et al.: Nanobob: a cubesat mission concept for quantum communication experiments in an uplink configuration. EPJ Quantum Technology. 5(6) (2018)

21. Andrews, L.C., Phillips, R.L.: Laser beam propagation through random media, ed. SPIE Press, Bellingham (2005)

22. Reeves, A.: Aotools Documentation April 2020. https://aotools.readthedocs.io/en/v1.0.1/

SUPPORTING INFORMATION

Additional supporting information may be found online in the Supporting Information section at the end of this article.